Prediction of orientation relationship and interface structure between α-, β-, γ-$FeSi_2$ and Si phases

M.A.Visotin*[a,b], I.A. Tarasov[a], A.S. Fedorov[a,b], S.N. Varnakov[a], S.G. Ovchinnikov[a,b]

[a]Kirensky Institute of Physics, Federal Research Center KSC SB RAS, Krasnoyarsk, 660036 Russia
[b]Siberian Federal University, 660041, Krasnoyarsk, Russia

*Corresponding author.
E-mail address: mav@iph.krasn.ru (Maxim A. Visotin).
Keywords: Interface structure; Structure Prediction; Orientation relationship; Near-coincidence site; Edge-to-edge matching; Iron silicide; DFT calculations; Thermal expansion;

Synopsis

Predictions of coherent interphase boundary orientations and atomic structures are carried out basing on purely crystallogeometric methods. Possible epitaxial interfaces are derived for α-, γ-, β-$FeSi_2$ and Si phases to verify the proposed approach and show prospects of disilicide heterojunctions synthesis.

Abstract

Pure crystallogeometric approach is proposed for predicting orientation relationships, habit planes and atomic structure of the interfaces between phases, which is applicable to systems of low-symmetry phases and epitaxial thin film growth. The suggested models are verified on the example of epitaxial growth of α-, γ-, β-$FeSi_2$ silicide thin films on a silicon substrate. The density of Near-Coincidence Sites is shown to have a decisive role in the determination of epitaxial thin film orientation and explains the superior quality of β-$FeSi_2$ thin grown on Si(111) over Si(001) substrates despite larger lattice misfits. Ideal conjunctions for interfaces between the silicide phases are predicted and this allows for utilisation of thin buffer α-$FeSi_2$ layer for oriented β-$FeSi_2$ nanostructures growth on Si(001). The thermal expansion coefficients are obtained within quasi-harmonic approximation from the DFT calculations in order to study influence of the temperature on the lattice strains in the interfaces. Faster decrease of misfits at α-$FeSi_2$(001)||Si(001) interface compared to γ-$FeSi_2$(001)||Si(001) elucidates the origins of temperature-driven change of the phase growing on silicon substrates. The proposed approach guides from bulk phase unit cells to the construction of the interface atomic structures and appears to be a powerful tool for the prediction of interfaces between arbitrary phases for subsequent theoretical investigation and epitaxial film synthesis.

1. Introduction

The physics of surfaces and interfaces contribute greatly to the properties of the materials in real applications, especially when miniaturisation and low-dimensional and nanostructures are considered. This includes a wide variety of effects, from Schottky barriers and electron scattering to topological materials [1–3]. Unlike the bulk properties, which are studied nowadays with a set of robust theoretical and experimental methods, investigation of structure and properties of the interfaces is yet a great challenge for materials science. Even the mechanisms defining possible orientation relationships (ORs) and habit planes (HP) between two phases are not fully known [4].

Most methods of searching for ORs between phases or at grain boundaries are purely geometric and originate from metallurgy, studying alloys, precipitation, and diffusional phase

transformations [5–12]. These methods are best at describing junctions between phases with quite similar high-symmetry structures, mainly fcc, hcp, bcc, and with a metallic type of chemical bonding, in that they are even capable of studying complex incoherent interface structures and defect distribution. However, in most cases, the description based on the matching of the lattice vectors is used, because in case of close-packed (cp) metal phases, matching of the lattice vectors from both phases almost definitely leads to good bonding between atoms within the unit cells and low interfacial energy. This is obviously not true for low-symmetry crystals [13], especially with more covalent-type of bonding, where matching of individual atomic sites and bonds should be obtained for minimisation of interfacial energy. Despite that, these methods have been successfully applied to epitaxial thin film synthesis of some cubic and hexagonal phases [14,15].

Nevertheless, it is still desirable to adapt such crystallogeometric methods for predicting ORs and HPs between more complex phases with the capability of taking into account the internal chemical bonding properties. In that, prediction of possible coherent interfaces with regular atomic structure is of great importance due to the stability of their electronic and transport properties on the one hand, and the compatibility of such substrate and film phases for epitaxial growth on the other hand. Feasibility of high-quality thin film synthesis is of particular interest for lattice strain band engineering [16,17] and for most of the applications in spintronics and optoelectronics. A vivid example of such case is an epitaxial synthesis of β-$FeSi_2$ on silicon substrates.

Semiconducting β-$FeSi_2$ phase can be utilised as the active material in photon crystals, photovoltaics, thermoelectrics and also for electric charge storage, while being of particular interest for light emission diodes (LED) [18–22]. However, many possible application opportunities are hindered by the poor quality of monocrystalline thin films, along with a lack of tunability and band control. E.g. the highest reported values for output optical power and external quantum efficiency of β-$FeSi_2$ devices are 420 μW and 0.12 % [23], respectively, which is currently inferior to that of InGaAs compounds [24]. Possible solutions in such cases are nanostructure growth and decreasing atomic structure defect density [25,26], but there are only a few reports of successful application of these approaches for β-$FeSi_2$ [27–29]. The most probable cause is high lattice mismatches between β-$FeSi_2$ and silicon [28,30].

The situation with β-$FeSi_2$ synthesis is also complicated by co-existence of other iron silicide phases (ferromagnetic metals Fe_3Si [31] and Fe_5Si_3 [32], and non-magnetic semiconductor ε-FeSi [33]), and especially isometric α-$FeSi_2$ [34], γ-$FeSi_2$ [28], and s-$FeSi_2$ [28] because the possibility of concurrent growth of several phases amplifies the role of interfacial energy. While the ORs of β-$FeSi_2$ growing on Si substrates have been quite deeply investigated [24], there is a lack of experimental data of preferable α-$FeSi_2$ and γ-$FeSi_2$ film orientations.

Yet, iron silicides-based nanostructures are attractive due to their ecological safety and Earth's core abundance that gives us the opportunity for a greener future with highly effective electronic devices. Also, such phase diagram peculiarities may give a possibility to control the morphology, lattice strain and, hence, the properties of the thin films by affecting the phase composition at the initial stages of the synthesis. While α-, γ- and s-$FeSi_2$ are growing in the form of separate nanocrystals, rather than homogenous thin films, which may be exploited for the self-assembled synthesis of different phase nanostructures atop these nanocrystals, e.g. β-$FeSi_2$ nanowhiskers. Thus, considering interfaces of different silicides with silicon and possible orientation relationship between them is of great interest.

Here, we present a unified approach, which not only predicts ORs and HPs between two crystal lattices but also accounts for the internal chemical structure of the phases and capable of proposing approximate atomic structures of the interfaces for further atomistic modelling. The proposed approach is described step-by-step in Section 2. In Section 3 it is used to systematically examine possible orientation relationships between silicon and disilicide phases and possibilities of high-quality film synthesis of the phases on different substrate orientations are discussed. In Section 4 temperature dependence of lattice strain due to misfits corresponding to the ORs is suggested as a driving force for the phase switch of the phase preferably growing at different temperatures.

2. Interface prediction approach

2.1 General description

Generally speaking, the question of finding the interfaces between two phases is a 10-D optimisation problem: the interfacial energy should be minimised with respect to 3 degrees of freedom (d.o.f.) corresponding to rotations of one crystal relative to another, 2 d.o.f. of habit plane orientations, 3 d.o.f. of translations of one crystal lattice relative to another, 1 d.o.f. corresponding to the position of interface region relative to the lattice of the crystals and 1 d.o.f. for interface thickness [35]. However, part of degrees of freedom may be reduced to a discrete number of variants by the adoption of some basic physics assumptions. If we are interested in coherent interfaces, strict periodicity in the interface is needed, which restricts the rotations of the lattices and HPs to those bringing lattice vectors into the interface plane. A requirement for an atomically sharp transition between the phases discards the value of interface thickness and restricts its position to the finite number of non-equivalent atomic sites. On the other hand, estimation of the interface energy is also a demanding task that can be done at different levels of complexity and accuracy, from full-scale electronic structure calculations to rough crystallogeometrical methods, like counting the number of coincidences and incoincidences of the sites in the conjugate lattices, which mimic the atomic defects in the interface.

Herein we focus on a purely geometrical approach to finding possible interfaces between α-, β-, γ-$FeSi_2$ and Si phases, which is simple enough to search through numerous variants and yet have already shown its efficiency. We use a systematic combination edge-to-edge matching method [7] to find possible ORs and subsequent near-coincidence sites (NCS) [11] density maximisation for prediction of the relative position of phases at the interface and also for comparison of different interfaces between each other. In that, a concept of atomic row density is reformulated to take into account small atomic displacements, which lies in the basement of the NCS matching, and thus both methods are used in a unified manner. Finally, the information about the coincidence sites is used to construct a simple atomistic model for the interface structure, which can be used as input for more advanced atomic structure prediction methods, e,g, dedicated Monte-Carlo, evolutionary or other heuristic algorithms [36,37] or directly in molecular dynamics or quantum-chemical studies.

The proposed approach gives a framework to construct possible interface structures basing only on the equilibrium crystal structures of the phases. The overall scheme of the approach is the following:

1. Find pairs of close-packed rows with low misfits;
2. Find ORs and HPs (relative orientation);
3. Stretch phases in accordance with the misfits;

4. Find highest NCS density (relative position);
5. Resolve the atomic structure of the interface.

2.2 Close-packed atomic rows

The ORs between phases are observed to be often guided by matching of close-packed atomic rows [7], which may be attributed to the need of correlated growth of the crystal phase across the interface. If the distance between the atomic sites in one lattice is sufficiently small, which means it is a close-packed (cp) row, this will promote coherent growth of the opposite phase [38]. Thus, the search for preferable ORs and HPs starts with determining the cp directions in the considered phases. Since in further considerations we assume that atoms are allowed to move around their equilibrium positions, we determine the packing density of a crystallographic direction by the number atoms lying within some distance from that line (a half of NCS criterion, 0.235 Å, see explanation in Section 2.5 below) divided by the length. The criterion of an atomic row to be close-packed is set to 0.1667 $Å^{-1}$, which corresponds to a maximum correlation distance between atomic sites to be 6 Å. This estimate was done based on the radial distribution function of amorphous silicon, which becomes monotonic at bigger radii [39].

2.3 Finding interface ORs

The approach we use in this work to predict the set of possible ORs of the interface between two phases is based on finding the good matching pairs of vectors of two crystals. The surface cell of the crystal is defined by two vectors $\mathbf{a_1}$ and $\mathbf{a_2}$ for the first phase, and $\mathbf{b_1}$ and $\mathbf{b_2}$ for the second phase (Fig. 1a). Initially, the array of all possible crystallographic translational vectors (including those of primitive cell) with the length of no more than Si[400] (21.7228 Å) is created. Such length maximum should not allow us to omit the possible direction pairs in the phases with the large difference in unite cell sizes, β-$FeSi_2$||Si, for instance. Then, the array generated is used to create a separate set of only symmetrically non-equivalent vectors by a filtering procedure, in which the symmetry operations (corresponding to point group of the phase) are applied to compare the vectors in the array and select only the unique ones. The array of all unique vectors in the crystal, within the restricted length range, besides the cp atomic rows, contains those ones with a very low atomic density. Thus, the atomic density was calculated for each direction in the array to exclude from the further consideration the loosely-packed atomic rows.

The next step aims to generate the array of surface unit cells for each phase. The first vector of the surface is always regarded as a close-packed and unique direction whereas the second vector is any vector in the crystal within the restricted length range. The generation of the surface cell array is conducted through the all-possible combinations between unique and non-unique vectors. However, symmetrically equivalent vector pairs are excluded so that to reduce the number of non-unique combinations at the next steps.

Further, the surface unit cells for each phase are combined to create the array of the interface orientation relationships. To determine possible good matching interfaces the filtration of the array obtained is applied regarding the vector misfit between the vectors of two surface unit cells (Fig. 1b). Vector misfits are defined as $\boldsymbol{\delta_1 = (|a_1| - |b_1|/|b_1|)*100\ \%}$, $\boldsymbol{\delta_1 = (|a_2 - b_2|/|b_2|)*100\ \%}$, $\mathbf{a_1}$ is the close packed vector length in the surface unit cell of first crystal, $\mathbf{b_1}$ refers to the second one, $\mathbf{a_2}$ and $\mathbf{b_2}$ refer to the second pair of any vector in the first and second phase, respectively.

For the criterion of maximal misfit value, a rather conservative value of 5 % was chosen, while the results for 4 and 7 % show good qualitative convergence, which is within typical misfit value range when one can expect epitaxial single crystal growth [40].

The final step is aimed to reduce the quantity of the interface ORs obtained by filtering out symmetrically equivalent ones. However, since the resulting interfaces will be subject to deformation, i.e. stretching/compressing strictly along the cp direction, only those symmetry operations are utilized, that conserve the direction of the first vector of the surface cell. For that, the rotation matrices aimed to locate the surface unit cells of each phase onto the XY plane of the Cartesian coordinate system, with the first cp vector parallel to X-axis, are calculated. Afterward, the corresponding symmetry operations are applied to the rotation matrices of all the ORs so that to compare them against each other. If any of these rotation matrices for both phases are equal for some pair of ORs, these orientation relationships were considered equivalent and one of them was removed.

2.4 Interface strains

For considering a candidate OR the lattice of one phase is stretched to fit the other one in the habit plane and thus construct a periodic interface structure. This is done by finding the matrix of transformation between the matching vector pairs and generally follows the same procedure as described in [41]. Despite that we cannot compare the interfacial and elastic energy contributions directly, we still estimate the magnitude of lattice deformation by decomposing the transformation matrix into rotation and deformation parts, and calculating the average strain same as in [41]:

$$\tilde{\varepsilon} = \frac{1}{2}\sqrt{\varepsilon_{xx}^2 + \varepsilon_{yy}^2 + \varepsilon_{xx}\varepsilon_{yy} + \varepsilon_{xy}^2}$$

where $\varepsilon_{\alpha\beta}$ are the components of the deformation matrix.

It worth noting that the NCS formalism does not imply stretching and fitting the lattices, however, the predictions of ORs favourability based on NCS density in unstrained interfaces do not correctly describe the experimental data on β-$FeSi_2$ growth on silicon substrates.

While the crystal lattices are subject to thermal expansion, the interface strains and misfits vary with the temperature. In order to analyse the role of this factor, the thermal expansion coefficients of the phases were obtained from Density Functional Theory (DFT) calculations using the quasi-harmonic approximation [42,43] and the temperature dependence of the corresponding interface strains was found. The results are presented in Section 4 and the details of calculation methods can be found in the Supplementary Information.

2.5 Optimising NCS density

Most of the crystallogeometric methods consider the atomic position strictly fixed to the lattice of the considered phases. But, like the phases are able to contract/stretch to accommodate to each other if the lattice mismatch is not very large, one should consider possibility of atoms move around their equilibrium positions. This idea was developed in the Near-Coincidence Site (NCS) matching approach [11].

Construction of the interface structures by site matching is based on the following idealistic model. If an atomic site of the phase #1, which falls into the interface region, coincides with an atomic site of the phase #2, such atomic site has the same type of neighbours as in either of the phases, and the bond lengths with these neighbours lie within the preferable range. This makes up good conditions for strong chemical bonding and, as a consequence, low interfacial energy, therefore the density of such matching atomic sites should be as high as possible. Of course, the matching atomic sites should correspond to the same or chemically analogous atomic species. Although regular ideal coincidence of atomic sites (as well as matching of the lattice periods) is almost impossible in reality, one may still consider two atomic sites matching if the distance between them is small enough to be compensated by possible atomic displacements.

An illustration of the NCS model is given in Fig. 1b. Two phases are intersecting in some interface region, the borders of which are shown with black solid lines. The near-coincidence sites between two phases, which are marked with arrows, are searched for within the interface region. The atomic sites, which do not coincidence with other or coincide with atoms of different chemical element, are considered not-matched sites and marked with "×" symbols.

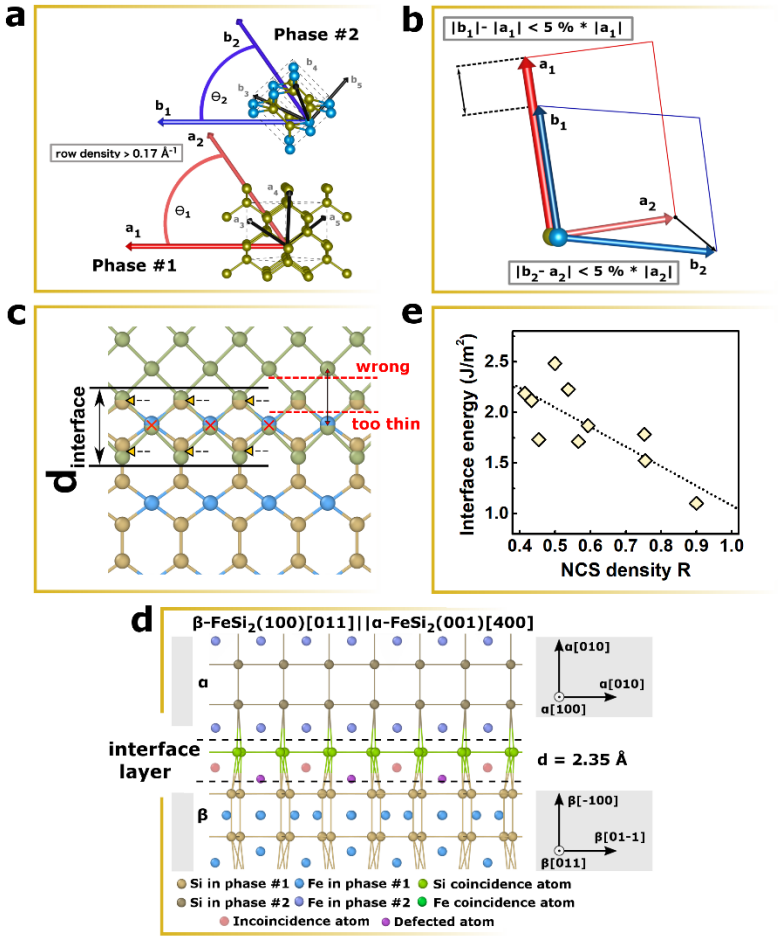

Figure 1
Illustration of the method finding a possible favourable ORs and atomic order on an interface (a) Search of the good matching surface unit cells of two crystals. (b) Scheme for calculation of misfit between two surface unit cell considered. (c) Schematic illustration of NCS atomic matching on an interface. (d) an example of automatically created atomic structure model for an interface between two crystals. (e) NCS density plotted VS interface energies calculated within DFT for some α||Si coherent interfaces.

Using this approach, different variants of two-phase conjunction may be compared by counting the number of such near-coincidence sites due to correspondence to the energy of

defects at the interface. If an atomic site of phase #1 at the interface is not matched by a site from phase #2, it would appear as a point defect, interstitial atom or vacancy if the site is occupied or not, respectively. Since phase #1 and phase #2 may have different atomic densities, it seems reasonable to search for the optimal interface structure by maximising the ratio of NCS to the overall number of the corresponding phase sites inside the interface region. Here, we use the following value to assess the goodness of the atomic site match:

$$R = \frac{1}{2}\left(\frac{m_1}{N_1} + \frac{m_2}{N_2}\right) \quad (1)$$

where N_1 and N_2 are the numbers of phase #1 and #2 atoms in the interface; m_1 and m_2 are the counts of near coincidence sites from the corresponding phases. The NCS density of the interface presented in Fig. 1b is R=2/3. In the right side of the figure, red dashed lines mark a model of the interface with R=1, but the interface region is too thin, which does not account for strong repulsion between the sites outside the interface being unphysically close to each other. While studying atomically sharp coherent interfaces, the thickness of the interface region should be kept as small as possible, but not less than the maximal bond length in the system to ensure that all bonds between the phases fall into the interface region. In our case, we use a thickness of 2.35 Å, which is Si-Si bond length.

To use the NSC density, one has to set the critical distance between two sites for them to be considered matching. The matching of the sites located at some distance is a result of the atoms' ability to move in the vicinity of equilibrium positions, which depends not only on the atomic species but the local environment, including possible point defects. As a rule, the maximal distance between two matching sites is chosen to be 10 % of the lattice parameter or 15-20 % of the nearest-neighbour distance and the exact value is said to have little impact on qualitative results. Herein, we have chosen a value of 0.47 Å (20 % of Si-Si bond length), which corresponds to a situation when two atoms have been moved 0.235 Å towards the common matching site. In that case the total deformation energy reaches 1.2 eV (in case of force constants equal 21 eV/Å^2 i.e. the maximal value among the considered phases found in DFT calculations in Section 4), which is not more than the point defect formation energy, e.g. 1.4-1.6 eV for a charged or neutral silicon vacancy in α-$FeSi_2$ [44]. Basing on the same considerations of allowed atomic displacements for an atom, we have altered the definition of close-packed atomic row sets. The atomic density of some crystallographic direction are determined by the number atoms lying within a distance of 0.235 Å from that line per period of translation.

In order to test the performance of R value criterion in assessing the energy of interphase boundaries, we selected 10 interfaces predicted by current approach for α-$FeSi_2$ and Si, calculated the interface energy (by means of DFT, see details in Supplementary Information) using the predicted atomic structures, and compared the energies against the values of R (Fig. 1d). With the correlation coefficient of 0.79 between the interface energy and the NCS density, the value of R proposed here appears to be a valid test for thermodynamic favourability of given interface formation, while being deduced from purely geometric considerations only.

In order to obtain the most favourable interface structure for a certain OR we have to maximise the NCS density R with respect to all possible translations of the phases relative to each other and to the interface. The vector of relative displacement should be defined modulo the translation vectors of either of the phases considered, so we use a 3D-mesh of vectors with a step of 0.15 Å and dimensions of 5.45×5.45×5.45 Å, which embrace either of Si, α-, and γ-$FeSi_2$ unit cells. For each relative displacement, a finite-size interface cell (100×100×2.35 Å) is built and filled with the interpenetrating lattices of the corresponding phases, and the number of NCS, as

well as the total number of atomic sites in the interface cell, is obtained to calculate the value of *R* for this displacement vector. After iterating over all the relative displacement vectors, the maximal possible NCS density *R* for considered OR and HP is found. The convergence of the results with respect to the 3D-mesh of displacement vectors used have been tested for the best 100 ORs: the results obtained with the step size of 0.15 Å have been checked against the results for the mesh with a step of 0.10 Å and good agreement between the values of *R* is observed.

2.6 Atomic configuration

The information about relative orientations and dispositions of the phases with respect to the HP is still insufficient to determine the atomic structure inside the interface region. One yet has to decide which of the lattice sites belonging to either of the phases are occupied. The question has to deal with the nature of chemical bonding and thus needs prior knowledge of favourable bond lengths (and, possibly, the chemical potentials of the elements, if some special synthesis conditions are concerned). Herein, we propose the following scheme for prediction of interface atomic structures between a substrate and epitaxially grown film:

First of all, the coincidence sites, i.e. places where analogous atomic species are situated in both phases, should be occupied by the atoms of the substrate species, due to their higher availability and stability. In the case of incoincidence sites, the minimisation of the interfacial energy requires that those sites should be occupied only if the energy of an interstitial atom defect is lower than a vacancy in that particular place. From a geometrical point of view, one can estimate whether the site is too close to other atoms in the system.

If an incoincidence site within the interface, originated from e.g. phase #1, is located too close to the atoms from the phases #2 across the interface, it may disrupt the local bonding order of the latter atom, which is in the position of its energetic minimum. So, placing atoms into incoincidence sites should be avoided unless they lay out of the 1st coordination sphere (2nd for BCC structures) from the atoms of the opposing phase. In case of disilicides, the critical distance of 2.82 Å has been chosen for this condition as it is outside the coordination spheres for the phases considered in the article and corresponds to a position of the secondary peak on RDF of amorphous silicon [39] just behind the main peak of nearest neighbours.

The critical distance between an incoincidence site and an atom from the interfacial region, which is not in the optimal local bonding environment, should be smaller. We have chosen the critical distance for this condition to be equal to the distance between the most energetically preferable interstitial defect site and the atoms of the crystal in β-$FeSi_2$, i.e. 2.2 Å before structural relaxation [44]. Summing up, if the incoincidence site is further than 2.2 Å from atoms inside the interface and further than 2.82 Å from atoms of opposing phase crystal, placing atom into this site is considered favourable, and such atoms are referred as “defected”.

It is also important to choose a priority between the types of incoincidence sites to settle the cases of the very close distance between them. Having lower bond angle stiffness, the metal atoms should be considered as more favourable for interstitial atom defects, than such covalent-type elements like silicon. Considering that, we adopt the following order: (Fe from the substrate) > (Fe from the film) > (Si from the substrate) > (Si from the film).

We would like to draw attention to the oversimplification used here, because the real global minimum interface structures may be much more complicated than what can be built based on the equilibrium lattice sites of the conjugate phases, and thus it is hardly possible to find them

from pure crystallogeometric approach. Nevertheless, the atomistic models obtained herein can be viewed as a first approximation, which can be used in further molecular dynamics or electronic structure investigations.

3. Interfaces in α-, β-, γ-$FeSi_2$ and Si phase systems

3.1 Predicted orientation relationships and interface structures of α-, β-, γ-$FeSi_2$ grown on silicon

Besides the most stable β-$FeSi_2$ phase, which has a base-centred orthorhombic structure with *Cmca* space group (a = 9.8764 Å, b = 7.7985 Å, and c = 7.8359 Å) [45], there are also the tetragonal α-$FeSi_2$ phase (*P4/mmm*, $a = b$ = 2.6955 Å, c = 5.1444 Å [46]), which is metastable in bulk samples, and a cubic phase occurring only in nanosized form, γ-$FeSi_2$ (*Fm-3m* CaF_2–type structure [28]). There is also a rarely reported s-$FeSi_2$ phase (*Pm-3m* [28]), which has a defected CsCl-type structure with partial Fe site occupancy and grows at low synthesis temperatures, i.e. at conditions far from the equilibrium. Therefore, we will consider herein only α-, β-, and γ-$FeSi_2$ phases and predict their ORs, HPs and interface structures with silicon.

First, the sets of the cp atomic rows in the phases were determined in accordance with the definition described above. The most close-packed direction in the silicide crystal lattices were found to be α[001], β[100] and γ[100], which is different from the results for the standard definition, based only on Bravais lattice type: α[010], β[110] and γ[110], respectively. The discrepancies of the two definitions are best illustrated on example of γ-$FeSi_2$ gamma phase where the 0.37113 $Å^{-1}$ linear packing of γ[100] corresponds to silicon cubic sublattice with spacing of 2.69 Å, while the shortest Bravais lattice γ[110] has the spacing of 3.81 Å. Matching atomic rows at the interface along the former direction is expected to have higher matching sites density than the latter. However, for the diamond cubic silicon phase the most close-packed direction is found to be Si[110] in both methods.

The full list of cp atomic rows and corresponding linear densities are given in Table S1 in Supplementary Information. According to the edge-to-edge method, these directions play a deterministic role in the silicide heteroepitaxy. Combinations of these sets of cp directions with any others were used to construct surface cells, which were then matched to obtain the ORs and HPs of all possible interfaces. After filtering out symmetrically equivalent ORs and those with the misfit values higher than the chosen critical value of 5 %, total numbers of interfaces were 4535, 556, 2559, 2713, 901 and 10571 for α-$FeSi_2$/Si, β-$FeSi_2$/Si, γ-$FeSi_2$/Si, α-$FeSi_2$/β-$FeSi_2$, γ-$FeSi_2$/β-$FeSi_2$, γ-$FeSi_2$/α-$FeSi_2$ respectively. The NCS densities R were calculated for all of these interfaces, and basing on them the ranking of favourable ORs was obtained. The topmost predicted orientation relationships and habit planes for the coherent interfaces between the phases are summarized in Table 1.

Table 1
Top of predicted high-R coherent interfaces between α-, β-, γ-$FeSi_2$ iron disilicide and Si phases. The habit planes (*hkl*) and close-packed directions [*uvw*] determining the orientation relationships are given, while the second pair of crystallographic vectors used for lattice matching are omitted for brevity. The references to experimental observation of such interfaces are given.

Ranking number	(hkl)	(hkl)	[uvw]	[uvw]	δ, close-	R, NCS	ε̃, strain,	References

					packed direction misfit, %	density	%	
	β-$FeSi_2$ || Si							
i.1	β(10-1)	Si(1-1-1)	β[010]	Si[110]	1.54	0.75	2.47	[24,47, 48]
i.2	β(-110)	Si(1-1-1)	β[001]	Si[110]	2.03	0.75	2.51	[24,47]
i.3	β(100)	Si(00-1)	β[010]	Si[110]	1.54	0.70	1.52	[47,49, 50]
i.7	β(-310)	Si(1-1-3)	β[002]	Si[220]	2.03	0.57	0.93	
i.8	β(-11-1)	Si(0-12)	β[011]	Si[200]	1.78	0.54	3.30	
i.9	β(-510)	Si(1-1-5)	β[001]	Si[110]	2.03	0.51	1.24	
i.10	β(00-1)	Si(1-10)	β[010]	Si[110]	1.54	0.48	4.65	[51,52]
	α-$FeSi_2$ || Si							
i.1	α(-112)	Si(1-1-1)	α[201]	Si[110]	-2.97	0.90	2.15	[48]
i.2	α(-2-14)	Si(1-1-3)	α[201]	Si[110]	-2.97	0.79	6.74	
i.3	α(1-1-1)	Si(1-1-3)	α[220]	Si[110]	-0.73	0.76	8.23	
i.4	α(00-1)	Si(00-1)	α[220]	Si[110]	-0.73	0.75	0.64	[53,54]
i.5	α(1-1-2)	Si(1-1-1)	α[220]	Si[110]	-0.73	0.75	2.15	[48]
i.6	α(010)	Si(00-1)	α[201]	Si[110]	-2.97	0.75	2.98	
i.24	α(1-1-2)	Si(1-10)	α[220]	Si[110]	-0.73	0.50	7.41	
	γ-$FeSi_2$ || Si							
i.1	γ(001)	Si(001)	γ[110]	Si[110]	-0.77	0.75	0.67	
i.2	γ(1-1-1)	Si(1-1-1)	γ[110]	Si[110]	-0.77	0.75	0.67	[48,55]
i.4	γ(1-1-3)	Si(1-1-3)	γ[110]	Si[110]	-0.77	0.59	0.67	
i.12	γ(0-13)	Si(001)	γ[100]	Si[100]	-0.77	0.51	2.03	
	β-$FeSi_2$ || α-$FeSi_2$							
i.1	β(001)	α(-110)	β[100]	α[002]	-4.01	1.00	1.81	
i.5	β(0-10)	α(-110)	β[100]	α[002]	-4.01	1.00	1.83	
i.7	β(100)	α(001)	β[011]	α[400]	2.53	1.00	2.14	
i.11	β(100)	α(010)	β[010]	α[201]	4.65	1.00	4.22	
i.17	β(-110)	α(1-1-2)	β[001]	α[220]	2.78	0.90	1.19	
	β-$FeSi_2$ || γ-$FeSi_2$							
i.1	β(100)	γ(001)	β[010]	γ[110]	2.33	1	2.17	
i.5	β(00-1)	γ(1-10)	β[010]	γ[110]	2.33	1	4.12	
i.9	β(-110)	γ(1-1-1)	β[001]	γ[110]	2.82	0.95	2.13	
i.28	β(10-1)	γ(1-1-1)	β[010]	γ[110]	2.33	0.54	2.04	
	α-$FeSi_2$ || γ-$FeSi_2$							
i.1	α(00-1)	γ(00-1)	α[220]	γ[110]	0.04	1.00	0.03	
i.3	α(010)	γ(00-1)	α[201]	γ[110]	-2.22	1.00	2.37	
i.7	α(1-10)	γ(1-10)	α[220]	γ[110]	0.04	1.00	2.37	
i.13	α(-1-12)	γ(1-1-1)	α[201]	γ[110]	-2.22	0.92	1.53	

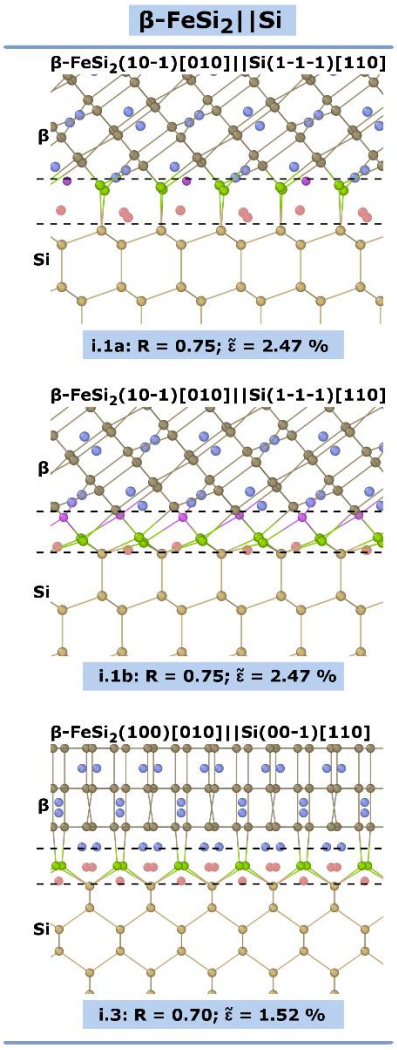

Figure 2
Predicted atomic structures for some epitaxial interfaces of β-$FeSi_2$||Si and corresponding NCS density *R* and interface strain ε̃. The borders of the interfaces are marked by dashed lines. The close-packed vectors [*uvw*] of the phases specified in square brackets are aligned along the view direction. For colour legend refer to Fig. 1d.

Among the predicted interfaces for β-$FeSi_2$ with Si, the highest *R* values correspond to Si{111} and Si{001} habit planes. The first couple of best-matching ORs, i.1 β(10-1)||Si(1-1-1) and i.2 β(-110)||Si(1-1-1), have *R* values of 0.75, ahead of the β(100)||Si(100) interface with *R*=0.7. Another technologically important silicon substrate plane Si(110) is presented utmost at the 10th position in the ranking by β(00-1)||Si(1-10) ORs, having *R*=0.48, which makes it less favourable for thin film growth. Although these interfaces contain the same pair of matching cp atomic rows Si[110]||β[010] with 1.54 % misfit, the second pairs of crystallographic vectors determining the ORs have different misfits and, as a result, the interface strain are rather different. β(100)||Si(100) has the lowest strain of $\tilde{\varepsilon}$=1.52 %, while the strain for β(10-1)||Si(1-1-1) is significantly higher, $\tilde{\varepsilon}$=2.47 %. Both values, *R* and $\tilde{\varepsilon}$, affect the possibility of interface formation; nevertheless, the experimental synthesis reports state that the β-$FeSi_2$ thin films grown on silicon (111), despite higher lattice misfits, exhibit better quality and higher structural stability in comparison to the films grown on Si(100), which tend to agglomerate in course of thermal treatment [50]. Therefore, it can be supposed that the NCS density is more important than the

interface strain and plays a decisive role in determination of orientation relationship of growing phases.

Moreover, possible interfaces of β-$FeSi_2$ with Si(110) substrate have much lower values of NCS density (R<0.48) and there are also several high-index habit planes with higher values R, which indicates possibility of formation of such facets instead of interface with Si(110). These facts agree well with the experimental observations of mainly endotaxial islands formation with other types of β||Si interface planes [56]. Also, the intrinsic presence of β(100) [011]/2 stacking faults at the interfaces of β(001) or β(010) facets parallel to substrate's inward Si(110) planes observed in β-$FeSi_2$ island formation [51] are explained with high interface strain value of 4.65 %. The high-quality β(010) thin film only obtained with preliminary activation of Si(110) surface with a thin silver layer [52]. Thus, the predictions for the β-$FeSi_2$||Si reproduce well the experimentally observed ORs with the same order of formation favourability, which argues for the applicability of the current approach to the silicide family compounds.

The stability of i.1 β(10-1)||Si(1-1-1) interface may be also assessed by predicted atomic structure. Within the same orientation relationship, two distinct types of atomic configuration corresponding to different relative displacements of the phases were found, both having R=0.75 (see Fig. 2 i.1a, i.1b). The presence of these two types appears due to two possible terminations of the Si(111) surface: the surface termination with a layer of single-coordinated atoms or 3-coordinated atoms. The interface i.1a is built by making the first type of atomic plane shared between the two phases and the resulting common silicon sites have tetrahedral (as in bulk Si) or triangular local environment. Making the second type of atomic plane shared results in a set of octahedrally coordinated silicon atoms at the i.1b interface. In addition to this, the i.1a interface may include some "defected" iron atoms, while in the i.1b interface part of silicon atoms from the β-$FeSi_2$ phase is treated as defected, because they do not find the coincident sites from Si, but there is enough space for them to be included in the interface. Also, both i.1 and i.2 interfaces are characterised with the rectangular symmetry of β(110), β(101) planes, that due to their superimposition with hexagonally symmetric Si(111) plane can potentially bring about the formation of three equivalent azimuthal orientation with the same atomic order on the interface during the β-$FeSi_2$ film growth.

The best-matching OR for Si(100) substrate, the i.3 β(100)||Si(100) interface has only one type of atomic structure with triangular coordination of Si atoms, and shows two variants of equivalent azimuthal orientation. However, two types of ORs are frequently reported [24]: i.3 corresponds to type A β-$FeSi_2$(100)[010]||Si(100)[011] and another OR, designated as type B β-$FeSi_2$ (100)[010]||Si(100)[001]. The type B OR was also found with the proposed methods, but the R value was rather low, 0.174, and therefore it is not presented in Table 1. In addition to this, it has larger interfacial strain of 3.65 %, which may be the cause of it less frequent appearance than type A.

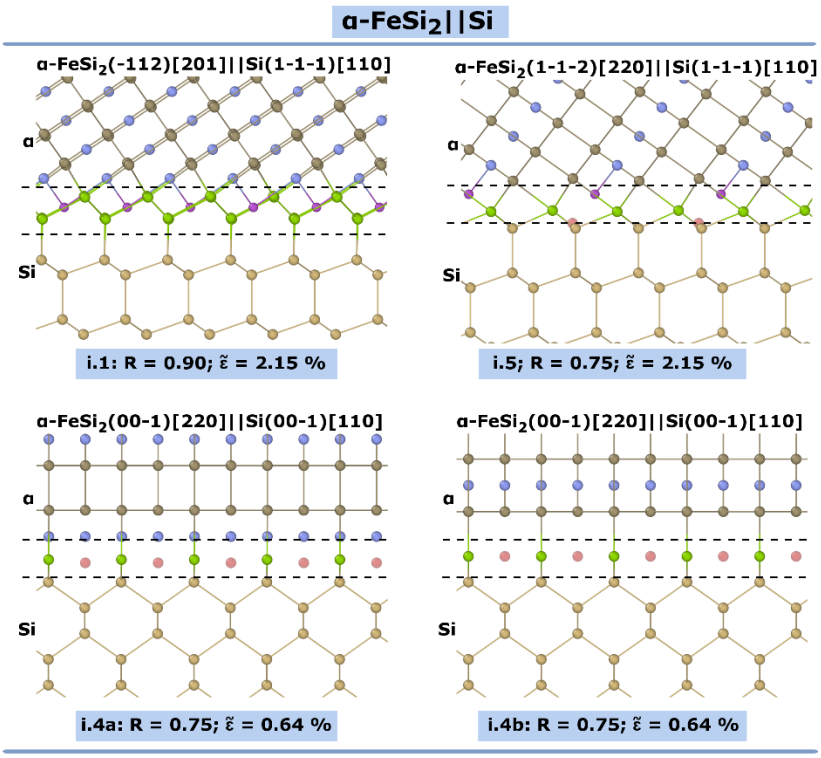

Figure 3
Predicted atomic structures for some epitaxial interfaces of α-$FeSi_2$||Si and corresponding NCS density *R* and interface strain ε̃. The borders of the interfaces are marked by dashed lines. The close-packed vectors [*uvw*] of the phases specified in square brackets are aligned along the view direction. For colour legend refer to Fig. 1d.

In case of α-$FeSi_2$ silicide epitaxy on silicon, the atomic row with the highest linear density, i.e. α[001], has too large misfit with Si[110], more than 7.2 %. The interface orientation of the phases are mainly guided by alignment of α[201] and α[220] cp atomic rows along Si[110], which exhibit low misfits of -2.98 % and -0.73 %. Thus, their combination gives us possible epitaxial interfaces with high NCS densities and rather low strains, $\tilde{\varepsilon}$=2.15 % for α||Si i.1 and α||Si i.5, $\tilde{\varepsilon}$=0.64 % for α||Si i.4.

The leading best-matching interface i.1 α(-112)[220]||Si(1-1-1)[110] corresponds to Si(111) habit plane, same as in case of β-$FeSi_2$||Si, however, the NCS density is significantly higher and the value of *R*=0.9 is the maximum among the silicide/silicon interfaces. There is also another α||Si(111) interface, i.5 α(1-1-2)[220]||Si(1-1-1)[110], with somewhat lower NCS density. This perfectly agrees with investigations of the epitaxial interfaces carried by I. Berbezier et al. in the early nineties with the help of high-resolution electron microscopy, which revealed these two types of the epitaxial relationships of the α-$FeSi_2$/Si(111) heterostructures [48]. The origin of differences in the *R* values can be found from comparison of the predicted interfaces atomic structures (Fig. 3 i.1, i.5). Silicon atoms at the i.5 interface have trigonal-prismatic coordination, which is not present in the bulk phases, while the i.1 interface consists of Si atoms with either tetrahedral or octahedral coordination, same as in cubic diamond lattice of silicon and bulk α-$FeSi_2$ structure, respectively. Also, both types have enough space in the interfacial region to host “defected” iron atoms.

The ORs of α-$FeSi_2$ growing on Si(001) substrate are presented by i.4 α(00-1)[220]||Si(00-1)[110] in the first place. This type of interface is characterized by 3-coordinated silicon atoms

and possibility of presence/absence of Fe atom layer inside α-$FeSi_2$ just next to the interface region, which is likely to affect the total interfacial energy (Fig. 3 i.4a, i.4b). It has R=0.75 and very low interfacial strain $\tilde{\varepsilon}$=0.64 %, which both argue for good ability of α-$FeSi_2$ to grow with such orientation relationship. Indeed, there is a set of reports on growth of such interfaces on Si(001) substrate by MBE or CVD methods [53,54]. At the same time, numerous experimental works show that this compound tends more to form free-standing nanocrystals partially embedded into silicon matrix [53,54,57–59], often with endotaxial α(112)||Si(111) interface formation, in compliance with the relative habit plane favourability order found herein. Presence of numerous high-index silicon planes among the topmost ORs (α||Si i.2, α||Si i.3, α||Si i.14, α||Si i.20) also suggests endotaxial growth of the α-$FeSi_2$ crystallites.

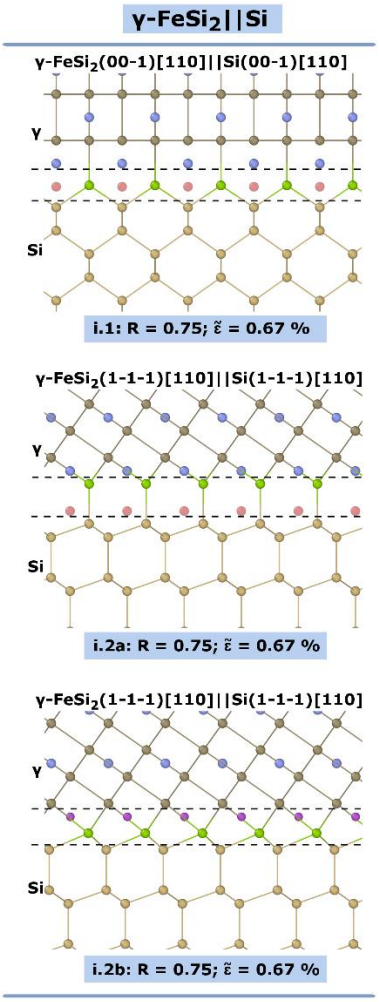

Figure 4
Predicted atomic structures for some epitaxial interfaces of γ-$FeSi_2$||Si and corresponding NCS density R and interface strain ε̃. The borders of the interfaces are marked by dashed lines. The close-packed vectors [*uvw*] of the phases specified in square brackets are aligned along the view direction. For colour legend refer to Fig. 1d.

The key directions for epitaxial alignment of γ-$FeSi_2$ and silicon are of the same type, i.e. γ[110] and Si[110], and also the ORs have mostly the same indices of the habit planes, which is a result of rather similar crystallographic groups: Fm-3m and Fd-3m for γ-$FeSi_2$ and Si,

respectively. The best-matching planes predicted to be i.1 γ(001)[110]||Si(001)[110] and i.2 γ(1-1-1)[110]||Si(1-1-1)[110], both having R=0.75 and $\tilde{\varepsilon}$=0.67 %, while the latter was previously reported among scarce experimental works on γ-$FeSi_2$ nanocrystal characterization [48,55]. As in case of β||Si i.1, γ(1-1-1)[110]||Si(1-1-1)[110] can be constructed with two possible atomic structures (Fig. 4 i.2a, i.2b), the former is characterised by hexagonal diamond lattice stacking, while the latter has trigonal-prismatic coordination of shared atom at the interface. The i.1 γ(001)[220]||Si(001)[110] has 3-coordinated Si atoms at the interface similar to the β||Si i.3 β(100)||Si(100) structure. Another ORs observed in experiment, γ(221)||Si(001) [60] was also predicted by current approach, although its NCS density is twice lower with R=0.32.

The interfaces of silicides with silicon cannot reach full matching of atomic sites at the interface (R=1.0) because of absence of Fe atom in silicon substrate phase. However, two silicide phases may have ideal atomic site coincidence at the interface. Also, possibility of concurrent growth of different silicide phases raises the question of possible silicide/silicide orientation relationships. Therefore, we have investigated ORs and the interfaces of α-$FeSi_2$||β-$FeSi_2$, γ-$FeSi_2$||β-$FeSi_2$ and γ-$FeSi_2$||α-$FeSi_2$.

3.2 Predicted interfaces of α-$FeSi_2$||β-$FeSi_2$, γ-$FeSi_2$||β-$FeSi_2$ and γ-$FeSi_2$||α-$FeSi_2$

γ-$FeSi_2$ phase is never observed in a form of continuous films as it is assumed to undergo a phase transition to β-$FeSi_2$ after reaching some critical size. Therefore the interface planes of γ-$FeSi_2$||β-$FeSi_2$ interfaces are interesting at the first place as the front of phase transformation. The most favourable interfaces, indeed, represent the same relative orientation relationship of the phases with different habit planes: i.1 γ(001)[110]||β(100)[010] and i.5 γ(1-10)[110]||β(001)[010], both with R=1. They are guided by alignment of γ[110] and β[010] cp directions, but the strain is lower for the γ||β i.1 than for γ||β i.5 interface: the values of $\tilde{\varepsilon}$ are 2.17 % and 4.12 % respectively. Despite similarity of crystal symmetry of γ-$FeSi_2$ and silicon, formation of interfaces with γ(111) plane is different from Si(111). The analogues of β||Si i.1 β(10-1)||Si(1-1-1) and i.2 β(-110)||Si(1-1-1) interfaces with R=0.75 have quite different NCS densities: i.9 γ(1-1-1)[110]||β(-110)[001] shows higher R=0.95, while i.28 γ(1-1-1)[110]||β(10-1)[010] has significantly lower R of 0.54.

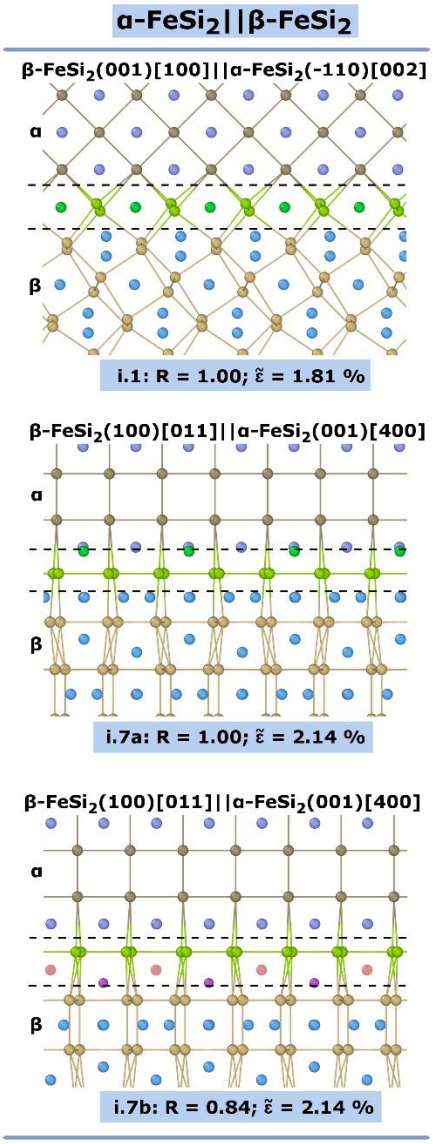

Figure 5
Predicted atomic structures for some epitaxial interfaces of α-$FeSi_2$||β-$FeSi_2$ and corresponding NCS density *R* and interface strain ε̃. The borders of the interfaces are marked by dashed lines. The close-packed vectors [*uvw*] of the phases specified in square brackets are aligned along the view direction. For colour legend refer to Fig. 1d.

The epitaxial interfaces of α-$FeSi_2$ and β-$FeSi_2$ phases are predicted to have four distinct types of ORs including i.1 α(-110)[002]||β(001)[100], i.5 α(-110)[002]||β(0-10)[100], i.7 α(001)[400]||β(100)[011] and i.11 α(010)[201]||β(100)[010], with interfacial strain values of 1.81 %, 1.83 %, 2.14 % and 4.22 %, respectively. The atomic structure of these interfaces (see Fig. 5) is characterised by sharing of either pure silicon or mixed silicon/iron atom layers, in which all Si atoms have 6 silicon neighbours with octahedral coordination, inherent to the bulk silicide phases. Thus, in case of co-existence, these two phases may have defect-free boundary between each other.

γ-$FeSi_2$||α-$FeSi_2$ interfaces have the lowest misfit among silicide||silicide conjunctions with full coincidence of sites: i.1 γ(00-1)[110]||α(00-1)[220] show R=1 and $\tilde{\varepsilon}$=0.03 %. Other types of ideal matching between the phases, although exhibiting much higher $\tilde{\varepsilon}$=2.37 %, include i.3 γ(00-

1)[110]||α(010)[201] and i.7 γ(1-10)[110]||α(1-10)[220]. It worth noting, if γ-$FeSi_2$ is grown on α-$FeSi_2$ as a substrate and then transforms to β-$FeSi_2$ according to the ORs found above, the orientation of resulting β-phase will be strictly correspondent to the most favourable β||α interfaces: i.1 γ||α will turn to i.7 α||β, i.3 γ||α will turn to i.11 α||β, and i.7 γ||α will turn to i.1 α||β.

Considering that the silicides show better ability to form coherent interfaces with each other rather than with silicon, one might utilize it to improve the quality of the thin films via layer-by-layer synthesis. The idea of growing β-$FeSi_2$ on Si substrate with a buffer layer of another silicide phase has been already suggested [61]. Herein, we observe that formation of β-$FeSi_2$(100) films atop Si(100) is hampered by low degree of interface site matching (R=0.7 for β||Si i.3) and rather high strain $\tilde{\varepsilon}$=1.52 %. Meanwhile the same silicon surface better facilitate formation of α-$FeSi_2$ with i.4 α(001)||Si(001) interface, which has R=0.75 and $\tilde{\varepsilon}$=0.64 %, and in turn, α(001) can host β-$FeSi_2$(100) film via ideally-matched i.7 α(001)||β(100) interface or γ-$FeSi_2$(001) i.1, which can grow into β-phase at large thickness. Such layer-by-layer synthesis is suggested to be suitable for growing highly oriented β-$FeSi_2$(100) film with internal stress due to lattice misfit with Si substrate, which is of great interest for band engineering applications [24,62].

In order to switch from growth of α-$FeSi_2$ to β-$FeSi_2$, a mechanism to control the preferable phase formation is needed. Along with deposition stoichiometry changing, which may affect the quality of the films and is difficult in case of disilicides growing on silicon, one should assess possibility of utilizing the temperature regimes to switch from one phase growth to another. Therefore, it is interesting to estimate the influence of thermal expansion on the characteristics of studied interfaces.

4. Temperature dependence of interface strain

The comparison of the ORs by the NCS density R presented above is related to the interfacial energy, which governs the growth of epitaxial films atop crystalline substrates. However, the growth is also affected by the elastic energy contribution, represented here by the interfacial strain $\tilde{\varepsilon}$, which in turn is greatly dependent upon the synthesis temperature due to lattice thermal expansion. This factor of different ORs occurrence was analysed by calculating corresponding values of $\tilde{\varepsilon}$ at different temperatures. The NCS density R is expected not to change with the temperature as long as the phases' structure factors have little dependence on temperature.

Little experimental data on the thermal expansion coefficients of α-$FeSi_2$ metastable silicide are reported, in particular, no studies on expansion anisotropy are available. As for γ-$FeSi_2$, the equilibrium lattice constant is not even known, because it was synthesised only in the form of nanosized precipitates inside the Si matrix. Therefore, we have used the values obtained within quasi-harmonic approximation (QHA) based on the DFT calculations, after comparing them against available experimental reports [64] [65,66]. The details of thermal expansion coefficient calculations and temperature-dependent lattice constants can be found in the Supplementary Information (Sections S2 and S3).

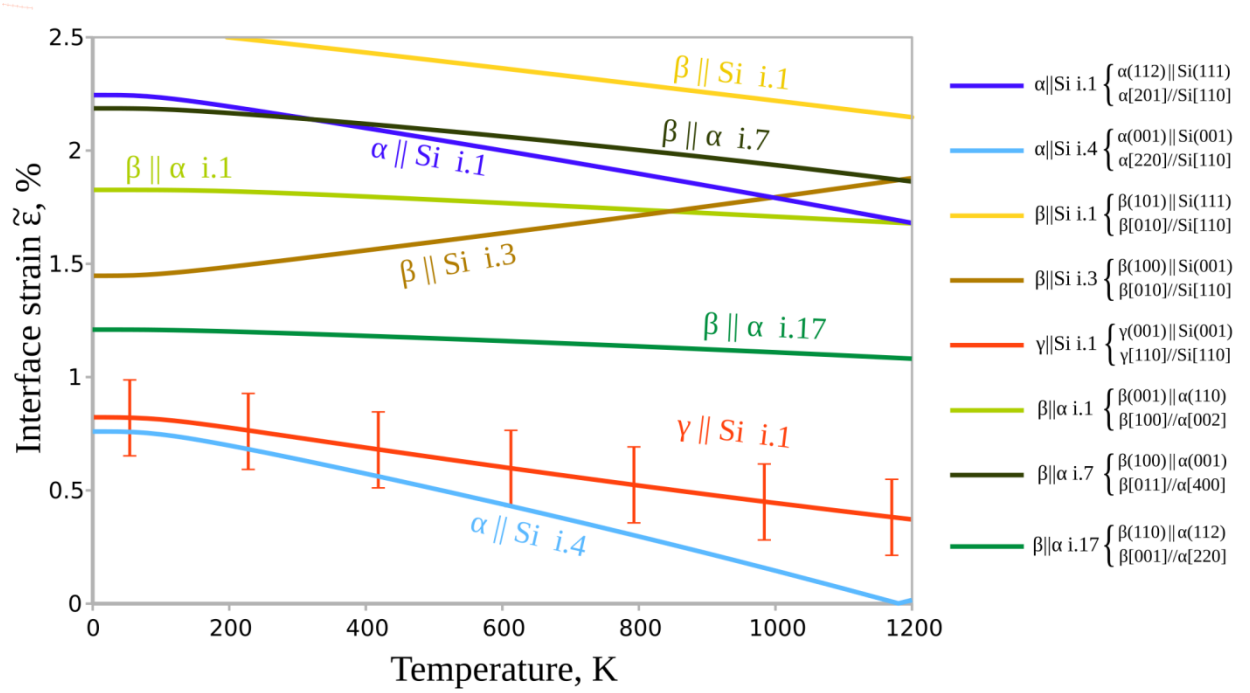

Figure 6
Temperature dependence of interface strain $\tilde{\varepsilon}$ for different silicon/silicide and silicide/silicide ORs from Table 1.

Due to its instability in the bulk, the real lattice constant of standalone γ-$FeSi_2$ is unknown, so we have estimated the interface strain basing on the theoretically calculated lattice constant for γ-$FeSi_2$. However, the DFT-PBE calculations usually tend to slightly underestimate the lattice constants compared to the experimental ones, e.g. by 0.36 % and 0.75 % for α-$FeSi_2$ and β-$FeSi_2$, respectively, thus we have corrected the values obtained for γ-$FeSi_2$ by 0.36-0.75 %, which corresponds to lattice constant estimate at 300 K in range of 5.375-5.396 Å. Therefore, the strain of the interface between γ and Si in Fig. 6. (γ||Si i.1) is presented with the range marks, corresponding to the upper and the lower limits of the correction.

As can be seen from Fig. 6 the effect of thermal expansion is most pronounced for the ORs of α||Si and β||Si. From the increase of β||Si i.3 interface strain, it can be concluded that β(100) films on Si(001) become less stable with the increase of temperatures, which agrees well with the experiment of film annealing [50]. The interfaces with Si(111) show the opposite behaviour: the strain decreases from 2.47 % to 2.22 % for β||Si i.1 with an increase of temperature from 300 K to 1000 K, which makes Si(111) a better substrate for β-$FeSi_2$ synthesis. Rather big thermal expansion coefficients of α-$FeSi_2$ favours high-temperature growth, because the strains are decreasing from 2.15 % to 1.79 % for α||Si i.1 and 0.64 % to 0.15 % (a fourfold decrease) for α||Si i.4 with increase of temperature from 300 K to 1000 K. The strains of different interfaces between the silicide phases are less dependent on the temperature, however the general trend for β||α strains is to decrease with temperature. The rest of interfaces, γ||β and γ||α are almost insensitive to thermal expansion, except for γ||α i.1, which increases from 0.09 % at room temperature to 0.39 % at T=1200 K.

At the room temperature, the strains of γ||Si i.1 and α||Si i.4 are approximately equal. Despite the uncertainty in the values of γ||Si i.1 interface strain, it is clearly seen that an increase of temperature leads to a much faster decrease in α||Si i.4 interface strain, which comes to 0 at

T=1200 K. As both interfaces have the same R=0.75, the growth of α-$FeSi_2$ should be expected at higher temperatures, which agrees well with the experimental reports on α-$FeSi_2$ formation at T>1000 K [66–68], while the growth of cubic γ-$FeSi_2$ is observed at lower temperatures [28,60,69–72]. Considering that γ-$FeSi_2$ undergoes a transition to β-$FeSi_2$ when the thickness of the film becomes larger than several nanometres, the elastic strain energy may be assumed to be the key factor of β→α phase growth switching at T=1000 K, which is much lower than their bulk phase transition temperature (1200 K).

Conclusions

Herein we propose a pure crystallogeometric approach for predicting orientation relationships, habit planes and atomic structure of the interfaces between phases, which is applicable to systems of low-symmetry phases and epitaxial thin film growth. The approach implies a systematic combination of the edge-to-edge matching method to find possible ORs and subsequent Near-Coincidence Sites density maximisation for assessing the quality of possible interfaces. Both methods are adapted to be used in a unified manner and complemented with a simple model of resolving the atomic structure of the interfaces between two phases.

The comparison of predicted ORs with the experimentally observed orientations for α- and β-$FeSi_2$ silicide thin films on silicon substrate show that the NCS density R can be utilised to compare interfacial energy of different ORs and, therefore, to estimate plausibility of high-quality epitaxial thin film growth on given substrates. In contrast, the lattice misfits or interface strains turn out to play only a secondary role in the determination of growing film orientation. Thus, the inferior quality of β-$FeSi_2$ films grown on Si(001) substrates in comparison to Si(111) can be explained in terms of lower value of R, although the magnitude of interfacial strain is lower for the case of Si(001) substrate. On the other hand, in the case of equal R values, the interfacial strain may be responsible for changing the $FeSi_2$ phase, which grows on the Si(001) surface. The temperature dependence of strain $\tilde{\varepsilon}$ obtained from DFT-calculated thermal expansion coefficients reveals that α-$FeSi_2$(001)||Si(001) OR favourability rises over γ-$FeSi_2$(001)||Si(001) with temperature increasing, which agrees well with experimental reports.

The orientation relationship of α-$FeSi_2$(112)||Si(111) is found to have the highest interfaces structure compatibility among all the silicide||silicon ORs having R equal 0.9, while in the other cases the values reach 0.75 at most. However, the interfaces between the silicides may show R=1.0, which corresponds to the ideal conjugation of the phase lattices. This fact can be utilised to achieve growth of high-quality oriented and strained semiconducting β-$FeSi_2$ nanostructures with a thin intermediate layer of α-$FeSi_2$ between the β phase and Si substrate, suitable for band-engineering and optoelectronic applications.

Overall, the proposed approach appears to be a powerful tool for prediction of ORs and the interface structures between arbitrary phases, which may be obtained by epitaxial growth techniques. While it demands only bulk crystal structure knowledge and, optionally, some prior knowledge on the bonging nature in the phases accessible by basic DFT calculations, the approach is suitable for the rapidly developing field of high-throughput computational material science investigations.

Funding information

This work was supported by the Russian Science Foundation, project no. 16-13-00060-П.

References

[1] K. Song, S. Ryu, H. Lee, T.R. Paudel, C.T. Koch, B. Park, et al., Direct imaging of the electron liquid at oxide interfaces, Nat. Nanotechnol. 13 (2018) 198–203. doi:10.1038/s41565-017-0040-8.

[2] D. Maccariello, W. Legrand, N. Reyren, K. Garcia, K. Bouzehouane, S. Collin, et al., Electrical detection of single magnetic skyrmions in metallic multilayers at room temperature, Nat. Nanotechnol. 13 (2018) 233–237. doi:10.1038/s41565-017-0044-4.

[3] F. Hellman, A. Hoffmann, Y. Tserkovnyak, G.S.D. Beach, E.E. Fullerton, C. Leighton, et al., Interface-induced phenomena in magnetism, Rev. Mod. Phys. 89 (2017) 025006. doi:10.1103/RevModPhys.89.025006.

[4] J.M. Howe, Structure, Composition and Energy of Solid–Solid Interfaces, in: Phys. Metall., Fifth Edit, Elsevier, 2014: pp. 1317–1451. doi:10.1016/B978-0-444-53770-6.00014-9.

[5] J.H. Van Der Merwe, G.J. Shiflet, P.M. Stoop, Structural ledges in interphase boundaries, Metall. Trans. A. 22 (1991) 1165–1175. doi:10.1007/BF02660648.

[6] Y. Champion, S. Hagege, An extended structural ledge description of heterophase interfaces, Interface Sci. 4 (1997) 191–203. doi:10.1007/BF00240241.

[7] M.X. Zhang, P.M. Kelly, Edge-to-edge matching and its applications: Part I. Application to the simple HCP/BCC system, Acta Mater. 53 (2005) 1073–1084. doi:10.1016/j.actamat.2004.11.007.

[8] A.R.S. Gautam, J.M. Howe, A method to predict the orientation relationship, interface planes and morphology between a crystalline precipitate and matrix. Part I. Approach, Philos. Mag. 91 (2011) 3203–3227. doi:10.1080/14786435.2011.573817.

[9] W.-Z. Zhang, G.C. Weatherly, On the crystallography of precipitation, Prog. Mater. Sci. 50 (2005) 181–292. doi:10.1016/j.pmatsci.2004.04.002.

[10] X. Wang, H. Huang, X. Gu, Y. Li, Z. Jia, Q. Liu, The orientation relationships of nanobelt-like Si 2 Hf precipitates in an Al–Si–Mg–Hf alloy, J. Appl. Crystallogr. 49 (2016) 1223–1230. doi:10.1107/S160057671600933X.

[11] Q. Liang, W.T. Reynolds, Determining interphase boundary orientations from near-coincidence sites, Metall. Mater. Trans. A. 29 (1998) 2059–2072. doi:10.1007/s11661-998-0032-2.

[12] F. Ye, W.Z. Zhang, D. Qiu, Near-coincidence-sites modeling of the edge facet dislocation structures of ?? precipitates in a Ti-7.26 wt.% Cr alloy, Acta Mater. 54 (2006) 5377–5384. doi:10.1016/j.actamat.2006.07.006.

[13] R.S. Hay, Orientation relationships between complex low symmetry oxides: Geometric criteria and interface structure for yttrium aluminate eutectics, Acta Mater. 55 (2007) 991–1007. doi:10.1016/j.actamat.2006.09.029.

[14] Z. Liu, Z. Zhang, R. Jiang, X. Li, M. Zhang, D. Qiu, Crystallography of phase transformation in the self-inclined InAs nanowires grown on GaAs{111}, Scr. Mater. 121 (2016) 79–83. doi:10.1016/j.scriptamat.2016.04.039.

[15] F. Wang, Y. Lei, D. Wang, Z. Lei, J. Sun, Z. Liu, On the growth morphology and crystallography of the epitaxial Cu 7 Te 4 /CdTe interface, CrystEngComm. 20 (2018) 1050–1056. doi:10.1039/C7CE02091K.

[16] R.J. Cottier, N.A. Steinle, D.A. Currie, N. Theodoropoulou, Band gap tuning of epitaxial SrTiO3-δ/Si(001) thin films through strain engineering, Appl. Phys. Lett. 107 (2015). doi:10.1063/1.4936608.

[17] O. Seo, A. Tayal, J. Kim, C. Song, Y. Chen, S. Hiroi, et al., Tuning of structural, optical band gap, and electrical properties of room-temperature-grown epitaxial thin films through the Fe2O3:NiO ratio, Sci. Rep. 9 (2019) 4304. doi:10.1038/s41598-019-41049-9.

[18] D. Leong, M. Harry, K.J. Reeson, K.P. Homewood, A silicon/iron-disilicide light-emitting diode operating at a wavelength of 1.5 μm, Nature. 387 (1997) 686–688. doi:10.1038/42667.

[19] H. Tokushige, T. Endo, K. Hiidome, K. Saiki, S. Kitamura, T. Katsuyama, et al., Photonic crystals composed of β-FeSi 2 with amorphous Si cladding layers, Jpn. J. Appl. Phys. 54 (2015) 07JB03. doi:10.7567/JJAP.54.07JB03.

[20] Z. Liu, S. Wang, N. Otogawa, Y. Suzuki, M. Osamura, Y. Fukuzawa, et al., A thin-film solar cell of high-quality -FeSi/Si heterojunction prepared by sputtering, Sol. Energy Mater. Sol. Cells. 90 (2006) 276–282. doi:10.1016/j.solmat.2005.03.014.

[21] M. Mohebali, Y. Liu, L. Tayebi, J.S. Krasinski, D. Vashaee, Thermoelectric figure of merit of bulk FeSi2-Si0.8Ge0.2 nanocomposite and a comparison with β-FeSi2, Renew. Energy. 74 (2015) 940–947. doi:10.1016/j.renene.2014.08.059.

[22] J. Theis, R. Bywalez, S. Küpper, A. Lorke, H. Wiggers, Charge storage in β -FeSi2 nanoparticles, J. Appl. Phys. 117 (2015). doi:10.1063/1.4906500.

[23] M. Suzuno, T. Koizumi, T. Suemasu, p-Si/β-FeSi2/n-Si double-heterostructure light-emitting diodes achieving 1.6 μm electroluminescence of 0.4 mW at room temperature, Appl. Phys. Lett. 94 (2009) 213509. doi:10.1063/1.3147168.

[24] D.Z. Chi, Semiconducting β-phase FeSi2 for light emitting diode applications: Recent developments, challenges, and solutions, Thin Solid Films. 537 (2013) 1–22. doi:10.1016/j.tsf.2013.04.020.

[25] M. Hetzl, M. Kraut, J. Winnerl, L. Francaviglia, M. Döblinger, S. Matich, et al., Strain-Induced Band Gap Engineering in Selectively Grown GaN–(Al,Ga)N Core–Shell Nanowire Heterostructures, Nano Lett. 16 (2016) 7098–7106. doi:10.1021/acs.nanolett.6b03354.

[26] L. Francaviglia, A. Giunto, W. Kim, P. Romero-Gomez, J. Vukajlovic-Plestina, M. Friedl, et al., Anisotropic-Strain-Induced Band Gap Engineering in Nanowire-Based Quantum Dots, Nano Lett. 18 (2018) 2393–2401. doi:10.1021/acs.nanolett.7b05402.

[27] S.-W. Hung, P.-H. Yeh, L.-W. Chu, C.-D. Chen, L.-J. Chou, Y.-J. Wu, et al., Direct growth of β-FeSi2 nanowires with infrared emission, ferromagnetism at room temperature and high magnetoresistance via a spontaneous chemical reaction method, J. Mater. Chem. 21 (2011) 5704. doi:10.1039/c1jm10232j.

[28] S. Liang, R. Islam, D.J. Smith, P.A. Bennett, Phase transformation in FeSi2 nanowires, J. Cryst. Growth. 295 (2006) 166–171. doi:10.1016/j.jcrysgro.2006.05.076.

[29] Q. Zhou, L. Liu, X. Gao, L. Chen, S. Senz, Z. Zhang, et al., Epitaxial growth of vertically free-standing ultra-thin silicon nanowires., Nanotechnology. 26 (2015) 075707. doi:10.1088/0957-4484/26/7/075707.

[30] G. Shao, Y. Gao, X.H. Xia, M. Milosavljević, Crystallographic characteristics and fine structures of semiconducting transition metal silicides, Thin Solid Films. 519 (2011)

8446–8450. doi:10.1016/j.tsf.2011.05.036.

[31] I. a. Tarasov, Z.I. Popov, S.N. Varnakov, M.S. Molokeev, A.S. Fedorov, I. a. Yakovlev, et al., Optical characteristics of an epitaxial Fe3Si/Si(111) iron silicide film, JETP Lett. 99 (2014) 565–569. doi:10.1134/S0021364014100105.

[32] S.G. Ovchinnikov, S.N. Varnakov, S.A. Lyashchenko, I.A. Tarasov, I.A. Yakovlev, E.A. Popov, et al., Iron silicide-based ferromagnetic metal/semiconductor nanostructures, Phys. Solid State. 58 (2016) 2277–2281. doi:10.1134/S1063783416110299.

[33] K. Ishizaka, T. Kiss, T. Shimojima, T. Yokoya, T. Togashi, S. Watanabe, et al., Ultraviolet laser photoemission spectroscopy of FeSi: Observation of a gap opening in density of states, Phys. Rev. B. 72 (2005) 233202. doi:10.1103/PhysRevB.72.233202.

[34] B. Aronsson, D.H. Templeton, S. Rundqvist, E. Varde, G. Westin, A Note on the Compositions and Crystal Structures of MnB2, Mn3Si, Mn5Si3, and FeSi2., Acta Chem. Scand. 14 (1960) 1414–1418. doi:10.3891/acta.chem.scand.14-1414.

[35] P.R.M. van Beers, V.G. Kouznetsova, M.G.D. Geers, M.A. Tschopp, D.L. McDowell, A multiscale model of grain boundary structure and energy: From atomistics to a continuum description, Acta Mater. 82 (2015) 513–529. doi:10.1016/j.actamat.2014.08.045.

[36] B. Gao, P. Gao, S. Lu, J. Lv, Y. Wang, Y. Ma, Interface structure prediction via CALYPSO method, Sci. Bull. 64 (2019) 301–309. doi:10.1016/j.scib.2019.02.009.

[37] A.L.S. Chua, N.A. Benedek, L. Chen, M.W. Finnis, A.P. Sutton, A genetic algorithm for predicting the structures of interfaces in multicomponent systems, Nat. Mater. 9 (2010) 418–422. doi:10.1038/nmat2712.

[38] B.. Joyce, D.. Vvedensky, A.. Avery, J.. Belk, H.. Dobbs, T.. Jones, Nucleation mechanisms during MBE growth of lattice-matched and strained III–V compound films, Appl. Surf. Sci. 130–132 (1998) 357–366. doi:10.1016/S0169-4332(98)00084-1.

[39] S. Kugler, G. Molnár, G. Petö, E. Zsoldos, L. Rosta, A. Menelle, et al., Neutron-diffraction study of the structure of evaporated pure amorphous silicon, Phys. Rev. B. 40 (1989) 8030–8032. doi:10.1103/PhysRevB.40.8030.

[40] S.R. Singamaneni, J.T. Prater, J. Narayan, Multifunctional epitaxial systems on silicon substrates, Appl. Phys. Rev. 3 (2016) 031301. doi:10.1063/1.4955413.

[41] L. Jelver, P.M. Larsen, D. Stradi, K. Stokbro, K.W. Jacobsen, Determination of low-strain interfaces via geometric matching, Phys. Rev. B. 96 (2017) 085306. doi:10.1103/PhysRevB.96.085306.

[42] L.L. Boyer, Calculation of Thermal Expansion, Compressiblity, an Melting in Alkali Halides: NaCl and KCl, Phys. Rev. Lett. 42 (1979) 584–587. doi:10.1103/PhysRevLett.42.584.

[43] R.E. ALLEN, F.W. DE WETTE, A. RAHMAN, Calculation of Dynamical Surface Properties of Noble-Gas Crystals. II. Molecular Dynamics, Phys. Rev. 179 (1969) 887–891. doi:10.1103/PhysRev.179.887.

[44] J. Chai, C. Ming, X. Du, P. Qiu, Y.-Y. Sun, L. Chen, Thermodynamics, kinetics and electronic properties of point defects in β-FeSi 2, Phys. Chem. Chem. Phys. 21 (2019) 10497–10504. doi:10.1039/C9CP00755E.

[45] H. Yamane, T. Yamada, Effects of stacking fault on the diffraction intensities of β-FeSi2, J. Alloys Compd. 476 (2009) 282–287. doi:10.1016/j.jallcom.2008.08.078.

[46] W. Miiller, J.M. Tomczak, J.W. Simonson, G. Smith, G. Kotliar, M.C. Aronson, Protected Fe valence in quasi-two-dimensional α -FeSi 2, J. Phys. Condens. Matter. 27 (2015) 175601. doi:10.1088/0953-8984/27/17/175601.

[47] J.E. Mahan, V. Le Thanh, J. Chevrier, I. Berbezier, J. Derrien, R.G. Long, Surface electron-diffraction patterns of β-FeSi2 films epitaxially grown on silicon, J. Appl. Phys. 74 (1993) 1747–1761. doi:10.1063/1.354804.

[48] I. Berbezier, J. Chevrier, J. Derrien, High-resolution electron microscopy study of α□FeSi2 heteroepitaxy on Si(111), Surf. Sci. 315 (1994) 27–39. doi:10.1016/0039-6028(94)90538-X.

[49] K. Konuma, J. Vrijmoeth, P.M. Zagwijn, J.W.M. Frenken, E. Vlieg, J.F. Van Der Veen, Formation of epitaxial β-FeSi2 films on Si(001) as studied by medium-energy ion scattering, J. Appl. Phys. 73 (1993) 1104–1109. doi:10.1063/1.353273.

[50] T. Suemasu, K. Takakura, C. Li, Y. Ozawa, Y. Kumagai, F. Hasegawa, Epitaxial growth of semiconducting β-FeSi2 and its application to light-emitting diodes, Thin Solid Films. 461 (2004) 209–218. doi:10.1016/j.tsf.2004.02.075.

[51] N. Jedrecy, Y. Zheng, A. Waldhauer, M. Sauvage-Simkin, R. Pinchaux, Epitaxy of β-<math display="inline"> <mrow> <msub> <mrow> <mi mathvariant="normal">FeSi</mi> </mrow> <mrow> <mn>2</mn> </mrow> </msub> </mrow> </math> on Si(111), Phys. Rev. B. 48 (1993) 8801–8808. doi:10.1103/PhysRevB.48.8801.

[52] K. Akiyama, H. Funakubo, M. Itakura, Epitaxial growth of (010)-oriented β-FeSi2 film on Si(110) substrate, MRS Proc. 1493 (2013) mrsf12-1493-e19-37. doi:10.1557/opl.2013.407.

[53] I.A. Tarasov, I.A. Yakovlev, M.S. Molokeev, M.V. Rautskii, I.V. Nemtsev, S.N. Varnakov, et al., Growth of α-FeSi<inf>2</inf>nanocrystals on si(100) with Au catalyst, Mater. Lett. 168 (2016). doi:10.1016/j.matlet.2016.01.033.

[54] R.V. Pushkarev, N.I. Fainer, H. Katsui, V.V. Kaichev, T. Goto, Structural features and surface composition of epitaxial α-FeSi 2 films obtained by CVD, Mater. Des. 137 (2018) 422–429. doi:10.1016/j.matdes.2017.10.030.

[55] I. Goldfarb, Synthesis of ultrathin semiconducting iron silicide epilayers on Si(111) by high-temperature flash, Surf. Sci. 554 (2004) L87–L93. doi:10.1016/j.susc.2004.02.012.

[56] Z.Q. Zou, X. Li, X.Y. Liu, K.J. Shi, X.Q. Guo, Thermal stability of iron silicide nanowires epitaxially grown on Si(110) substrates, Appl. Surf. Sci. 399 (2017) 200–204. doi:10.1016/j.apsusc.2016.12.056.

[57] J.K. Tripathi, G. Markovich, I. Goldfarb, Self-ordered magnetic α-FeSi2 nano-stripes on Si(111), Appl. Phys. Lett. 102 (2013) 251604. doi:10.1063/1.4812239.

[58] S.Y. Chen, H.C. Chen, L.J. Chen, Self-assembled endotaxial α-FeSi2 nanowires with length tunability mediated by a thin nitride layer on (001)Si, Appl. Phys. Lett. 88 (2006) 2004–2007. doi:10.1063/1.2202701.

[59] I.A. Tarasov, M.A. Visotin, A.S. Aleksandrovsky, N.N. Kosyrev, I.A. Yakovlev, M.S. Molokeev, et al., Si/Fe flux ratio influence on growth and physical properties of polycrystalline beta-FeSi 2 thin films on Si(100) surface, J. Magn. Magn. Mater. 440 (2017) 144–152. doi:10.1016/j.jmmm.2016.12.084.

[60] I. Goldfarb, Y. Camus, M. Dascalu, F. Cesura, R. Chalasani, A. Kohn, Tuning magnetic

response of epitaxial iron-silicide nanoislands by controlled self-assembled growth, Phys. Rev. B. 96 (2017) 045415. doi:10.1103/PhysRevB.96.045415.

[61] Y. Gao, G. Shao, R.S. Chen, Y.T. Chong, Q. Li, TEM study of self-assembled FeSi2 nanostructures by ion beam implantation, Solid State Commun. 149 (2009) 97–100. doi:10.1016/j.ssc.2008.11.002.

[62] R. Shao, K. Zheng, B. Wei, Y. Zhang, Y. Li, X. Han, et al., Bandgap engineering and manipulating electronic and optical properties of ZnO nanowires by uniaxial strain, Nanoscale. 6 (2014) 4936–4941. doi:10.1039/C4NR00059E.

[63] R.L. Maltez, M. Behar, X.W. Lin, Ion-beam induced sequential epitaxy of α, β and γ-FeSi2 in Si (100) at 320°C, Nucl. Instruments Methods Phys. Res. Sect. B Beam Interact. with Mater. Atoms. 106 (1995) 400–403. doi:10.1016/0168-583X(95)00739-3.

[64] M. Imai, Y. Isoda, H. Udono, Thermal expansion of semiconducting silicides β-FeSi2 and Mg2Si, Intermetallics. 67 (2015) 75–80. doi:10.1016/j.intermet.2015.07.015.

[65] F. Zhang, S. Saxena, Phase stability and thermal expansion property of FeSi2, Scr. Mater. 54 (2006) 1375–1377. doi:10.1016/j.scriptamat.2005.11.076.

[66] C. Detavernier, C. Lavoie, J. Jordan-Sweet, A.S. Özcan, Texture of tetragonal <math display="inline"> <mi>α</mi> <mo>−</mo> <mrow> <msub> <mrow> <mi mathvariant="normal">FeSi</mi> </mrow> <mrow> <mn>2</mn> </mrow> </msub> </mrow> </math> films on Si(001), Phys. Rev. B. 69 (2004) 174106. doi:10.1103/PhysRevB.69.174106.

[67] G. Cao, D.J. Singh, X.-G. Zhang, G. Samolyuk, L. Qiao, C. Parish, et al., Ferromagnetism and Nonmetallic Transport of Thin-Film α−FeSi2 : A Stabilized Metastable Material, Phys. Rev. Lett. 114 (2015) 147202. doi:10.1103/PhysRevLett.114.147202.

[68] I.A. Tarasov, I.A. Yakovlev, M.S. Molokeev, M.. Rautskii, I.V. Nemtsev, S.N. Varnakov, et al., Growth of α-FeSi2 nanocrystals on si(100) with Au catalyst, Mater. Lett. 168 (2016) 90–94. doi:10.1016/j.matlet.2016.01.033.

[69] H. Von Känel, K.A. Mäder, E. M̈ller, N. Onda, H. Sirringhaus, Structural and electronic properties of metastable epitaxial $FeSi_{1+x}$ films on Si(111), Phys. Rev. B. 45 (1992) 13807–13810. doi:10.1103/PhysRevB.45.13807.

[70] H. von Känel, N. Onda, H. Sirringhaus, E. Müller-Gubler, S. Goncalves-Conto, C. Schwarz, Epitaxial phase transitions in the iron/silicon system, Appl. Surf. Sci. 70–71 (1993) 559–563. doi:10.1016/0169-4332(93)90579-Z.

[71] A.L.V. de Parga, J. de la Figuera, C. Ocal, R. Miranda, A new metastable epitaxial silicide: FeSi2/Si(111), Ultramicroscopy. 42–44 (1992) 845–850. doi:10.1016/0304-3991(92)90367-S.

[72] D. Das, J.C. Mahato, B. Bisi, B. Satpati, B.N. Dev, Self-organized patterns along sidewalls of iron silicide nanowires on Si(110) and their origin, Appl. Phys. Lett. 105 (2014) 191606. doi:10.1063/1.4901815.